1 **The Fate of Sediment After a Large Earthquake**

2 **Oliver Francis[1,2,*], Xuanmei Fan[3], Tristram Hales[1,2], Daniel Hobley[2], Qiang Xu[3], Runqiu**
3 **Huang[3]**

4 [1]Sustainable Places Research Institute, Cardiff University, Cardiff, United Kingdom

5 [2]School of Earth and Environmental Sciences, Cardiff University, Cardiff, United Kingdom

6 [3]State Key Laboratory for Geohazard Prevention and Geoenvironment Protection, Chengdu
7 University of Technology, Chengdu, China

8 Corresponding author: Oliver Francis (Oliver.Francis@gfz-potsdam.de)

9 *Now at Section 4.7: Earth Surface Process Modelling, German Research Centre for
10 Geosciences (GFZ), Potsdam, Germany

11 **Key Points:**

12 - Significant volumes of sediment produced by the 2008 M_w7.9 Wenchuan earthquake
13   remain on the hillslope 10 years after the event.

14 - Debris flows rather than fluvially driven erosion are the key process in transporting
15   sediment from the hillslope into the main river.

16 - The decrease in debris flows frequency in the decade since 2008 is coincident with an
17   order of magnitude reduction in sediment export.

18 **Abstract**

19 Large earthquakes cause rapid denudation of hillslopes by triggering thousands of coseismic
20 landslides. The sediment produced by these landslides is initially mobilised out of the landscape
21 as a cascade of unknown magnitude. This cascade dramatically enhances local erosion rates
22 before rapidly returning to pre-earthquake levels. Identifying the individual processes of this
23 cascade and estimating the volume of sediment they mobilise is crucial to determining the
24 timescales over which earthquakes can influence hazards and sedimentary systems. Here we
25 present a fully constrained sediment budget of the first decade after the 2008 M_w7.9 Wenchuan
26 earthquake. With this budget we identify the key erosion processes within the post seismic
27 sediment cascade and constrain estimates of the volume of sediment removed from the
28 landscape. With these estimates we find that over 90% of the coseismically generated sediment
29 remaining on the hillslope 10 years after the earthquake. Despite the large volumes of sediment
30 on the hillslope, we observe an order of magnitude decrease in the erosion rate of the epicentral
31 area. Debris flows are the key erosional mechanism of the coseismically generated sediment as
32 erosion rates are correlated with debris flow frequency. Erosion rates likely remain elevated for
33 several decades however, the rapid stabilisation of the sediment following the earthquake
34 suggests large volumes of coseismically generated sediment can remain in orogens for hundreds
35 or thousands of years. In the most tectonically active regions, the long residence times of
36 coseismically generated sediment could significantly reduce bedrock incision rates in channels
37 altering long term erosion rates.

38

39 **Plain Language Summary**

40 Earthquakes produce large volumes of sediment by triggering landslides in mountain ranges.
41 Immediately after an earthquake there is an order of magnitude increase in erosion rates,
42 however this period of enhanced erosion is short lived. Understanding the mechanisms which
43 control the timespan of the elevated erosion rates and the rates at which they move sediment is
44 vital for determining the continuing impact the earthquake has on the landscape. Using satellite
45 imagery to map and track the movement of sediment after the 2008 Wenchuan earthquake we
46 show that more than 90% of the sediment produced by the earthquake remains on the hillslope a
47 decade after the earthquake. Debris flows initiating in the landslide deposits are responsible for
48 most of the erosion during this time. The frequency of these flows decreases rapidly after the
49 earthquake reducing the overall erosion rates close to normal levels. The remaining sediment
50 could reside in the orogen for hundreds or thousands of years indicating that it could have a
51 significant impact on long term erosion rates and landscape evolution.
52

1 Introduction

Large, continental earthquakes can produce thousands of coseismic landslides mobilising several cubic kilometres of sediment from the hillslope (Keefer 2002; Malamud et al. 2004). Coseismic landsliding is likely to be a key erosional process in these regions, potentially accounting for over 50% of long term erosion rates (Li et al. 2014; Marc et al. 2016b; Marc et al. 2016a; Li et al. 2017). Understanding how earthquakes affect the evolution of landscapes requires a consideration of both the direct impact of the landslides on hillslopes and how the erosion or storage of the sediment impacts the evolution of the channel network (Egholm et al. 2013; Campforts et al. 2020). Coseismic landslides reduce the relief of steep hillslopes and can alter the size of drainage basins via erosion of basin ridges (Schmidt and Montgomery 1995; Dahlquist et al. 2018). While the landslide deposits contribute to debris flow generation (Fan et al. 2019b) and provide tools or cover for abrading/protecting the bedrock channels (Turowski and Rickenmann 2009; Yanites et al. 2010; Egholm et al. 2013) altering the evolution of upland rivers. Long term storage of the coseismically generated sediment can dampen the isostatic response of an earthquake (Densmore et al. 2012) or reduce the bedrock erosion of future earthquakes (Li et al. 2014; Marc et al. 2016b; Stolle et al. 2019; Francis et al. 2020). Therefore, to fully incorporate earthquakes into models of long-term landscape we must understand the processes and timescales by which coseismically generated sediment is exported from orogens. Key to this aim is fully understanding and quantifying the erosional processes of the coseismically generated processes following earthquakes.

Following large earthquakes it is typical (though not always (Tolorza et al. 2019)) to see an order of magnitude increase in sediment discharge in orogen draining rivers (Pain and Bowler 1973; Hovius et al. 2000; Dadson et al. 2004; Hovius et al. 2011; Wang et al. 2015). However, this period of elevated erosion is generally short lived, typically less than a decade, resulting in significant, but unquantified, volumes of sediment remaining in the orogen after sediment discharges have returned to previous levels. As many coseismic landslides occur in bedrock much of the sediment within their deposits is too coarse to be transported by suspension resulting in aggradation of channels for decades after an earthquake (Pearce and Watson 1986; Koi et al. 2008; Vanmaercke et al. 2017). This coarse sediment must be transported by bedload processes and is likely to remain in the landscape for hundreds of years. Empirical estimates of bedload transport estimate that the sediment from the 1999 Chi Chi earthquake in Taiwan could take 250-600 years to be fully evacuated from the landscape (Yanites et al. 2010). Detailed dating and mapping of the Pokhara region in Nepal also suggests river system can rework sediment from large earthquakes for several hundred years (Schwanghart et al. 2016; Stolle et al. 2017; Stolle et al. 2019).

Alongside the residence time of sediment in the fluvial system, we must also consider possible storage of sediment on the hillslope. Small landslide deposits can be deposited on the hillslope far from the river or deposited in channels which lack the discharge to consistently erode them (Pearce and Watson 1986; Li et al. 2016; Roback et al. 2018). Landslides disconnected from the channel network cannot be actively reworked by undercutting and therefore must be eroded into the channel network by diffusive processes or stochastically by debris flows, which could significantly increase their residence times (Vanmaercke et al. 2014; Zhang and Zhang 2017; Fan et al. 2019b). Attempting to include connectivity in dynamic models of sediment transport is difficult due to the rates and initiation mechanisms of these processes being unknown in many

99   locations. However, simple statistical numerical modelling suggests that unconnected landslide
100   deposits could extend the period of time impacted by the earthquake by hundreds or thousands of
101   years (Croissant et al. 2019; Francis et al. 2020).
102
103   Satellite imagery with high spatial and temporal resolution allows for the monitoring of large
104   areas of mountain ranges. These can be used to generate multi-temporal landslide inventories
105   after major earthquakes to understand the spatio-temporal evolution of post seismic mass wasting
106   processes (Marc et al. 2015; Tang et al. 2016; Zhang and Zhang 2017; Kincey et al. 2021).
107   Multi-temporal inventories can provide a link between long term sedimentary (Stolle et al. 2019)
108   and short term suspended sediment discharge records (Lin et al. 2008) by helping to identify the
109   key sediment transport processes. Here we use a multitemporal landslide inventory of the 2008
110   Mw 7.9 Wenchuan earthquake to generate the first sediment budget of a large earthquake. We
111   use this sediment budget to determine the key sediment transport processes in the post seismic
112   landscape and to pose questions about the long-term evolution of the epicentral area.
113

114   1.2 The Longmen Shan and the 2008 M$_w$7.9 Wenchuan earthquake
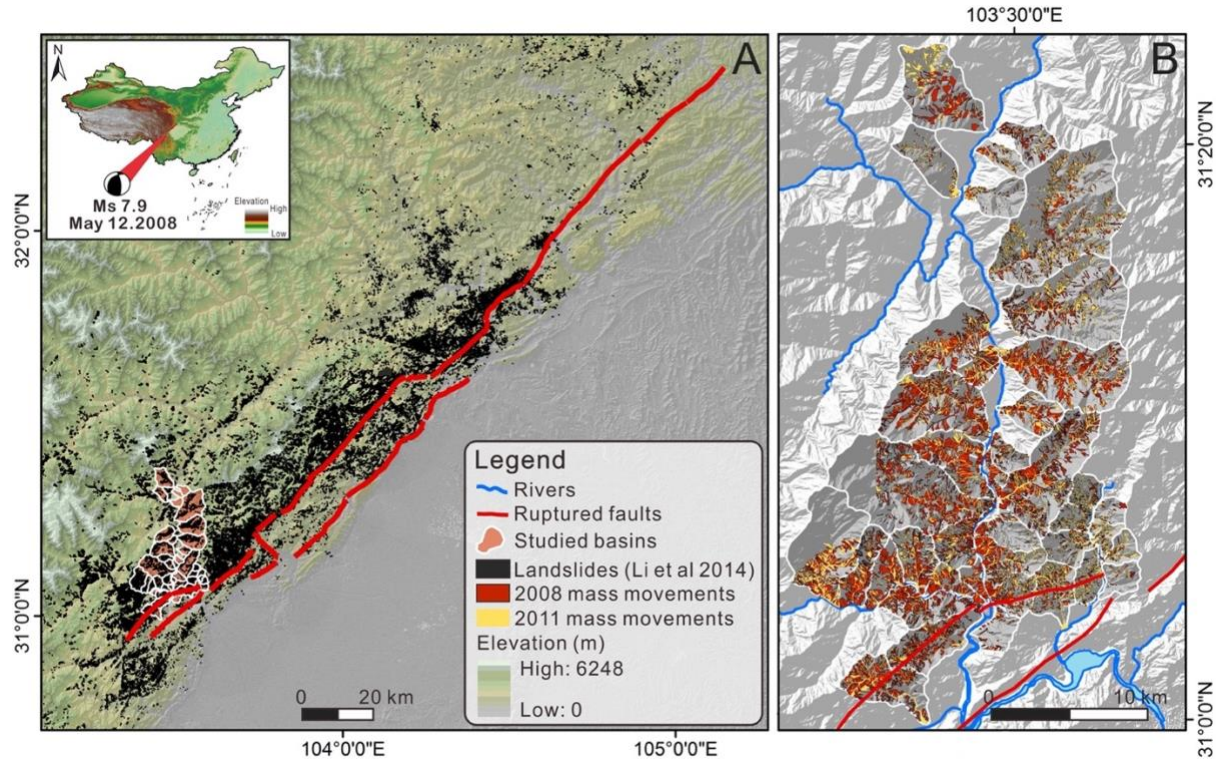

115
116   **Figure 1.** A) The surface rupture of the earthquake in red with the landslides in black. Note the
117   highest densities of landslides area found close to the ruptures. The inset shows the location of
118   the earthquake on the eastern margin of the Tibetan Plateau and the edge of the Sichuan Basin.
119   The catchments highlighted in white are the catchments studied in this paper. B) The studied
120   catchments with the Min Jiang running north to south through the middle of the image. The
121   coseismic mass movements are mapped in red while the post seismic (between 2008 and 2011)
122   movements are in yellow.

123
124   On the 12th May 2008 the country of Wenchuan in the Chinese province of Sichuan was shaken
125   by a magnitude M_w7.9 earthquake. The earthquake occurred along the Longmen Shan thrust
126   zone, which separates the Longmen Shan mountain range from the Sichuan Basin, and ruptured
127   2 major faults for over a hundred kilometres (Figure 1) (Liu-Zeng et al. 2009; Densmore et al.
128   2010). The earthquake triggered more than 60,000 landslides across an area of 35,000 km^2
129   (Huang and Fan 2013; Li et al. 2014) making it one of the most erosive earthquakes on record
130   (Marc et al. 2016a). Coseismic landsliding is found in the greatest densities close to the traces of
131   the ruptured faults with areal densities of up to 9.6% (Dai et al. 2011). Areas around the fault
132   zone have weaker rock strength than expected of fresh bedrock (Gallen et al. 2015) and higher
133   denudation rates than the rest of the landscape, suggesting frequent earthquakes have conditioned
134   the area resulting in rapid erosion rates (Li et al. 2017).
135
136   The Longmen Shan is one of the steepest mountain ranges in the world, the frontal range rapidly
137   increases in elevation from 500 – 4000m over distances of just 50km (Kirby and Ouimet 2011).
138   The mountain range is the eastern margin of the Tibetan Plateau and as a result is an area of
139   complex tectonic and geodynamic activity (Burchfiel et al. 2008; Royden et al. 2008; Hubbard
140   and Shaw 2009). The high mountain peaks are dissected by deeply incised valleys and gorges of
141   the rivers draining the mountain range (Densmore et al. 2007; Kirby and Ouimet 2011). The Min
142   Jiang, the major river draining the epicentral area, is bordered with several layers of terraces
143   which record the long term uplift and incision of the area (Godard et al. 2010). The main trunk of
144   the river has a characteristic width of 100m while many of the tributary catchments which drain
145   into the river in the epicentral region of the earthquake are significantly smaller (Figure 2A).
146   Rainfall is highly variable across the mountain range with the highest annual precipitation (800 –
147   1200mm) found right on the mountain front (Guo et al. 2016). Rainfall and river discharge also
148   vary temporally, the monsoon season between May and October is responsible for the majority
149   of the rainfall and discharge (Wang et al. 2015). Mass movements are common in the Longmen
150   Shan due to the steep hillslopes and high frequency of intense rain storms in the mountain range
151   (Ouimet et al. 2007; Ouimet et al. 2009).
152
153   Following the earthquake coseismic landslide sediment immediately began to be remobilised and
154   reworked by the fluvial system. Suspended sediment discharges in the Min Jiang, and other
155   rivers, increased by an order of magnitude (Wang et al. 2015), while the concentrations of
156   cosmogenic ^{10}Be in detrital sediment dramatically declined (West et al. 2014; Wang et al. 2017).
157   On average these records show that sediment transport has or is returning rapidly to pre-
158   earthquake levels in the years since. However, there is significant variation in this pattern which
159   is primarily linked to the landslide density in individual catchments. Catchments with higher
160   landslide densities and more frequent large rainstorms tend to produce larger and longer lasting
161   increases in sediment discharge (Wang et al. 2015; Wang et al. 2017). These increases seem to
162   be unaffected by the volume of sediment connected to channel network. Around 40% of the total
163   coseismic landslide sediment volume is connected to the channel network but suspended
164   sediment discharge remains high even in locations with low connectivity (Li et al. 2016). The

165 lack of a correlation between suspended sediment discharge and connectivity could be an
166 indicator of the high mobility of fine sediment immediately after the earthquake.
167
168 The most striking indicator of the earthquake significantly impacting the sediment transport rates
169 of the area is the occurrence of huge (mobilising $>10^6$ m^3 of sediment) debris flows (Tang et al.
170 2012). These are some of the largest debris flows ever observed and have occurred with
171 frequencies rarely seen elsewhere (Korup 2012). The debris flows occurred in the smaller
172 tributary catchments of the Min Jiang where high landslide densities are common and significant
173 aggradation of the channel bed is observed (Zhang and Zhang 2017) (Figure 2b). These large
174 debris flows are the single largest part of the stochastic sediment cascades (Bennett et al. 2014;
175 Zhang and Zhang 2017). Understanding these events in the context of other smaller processes in
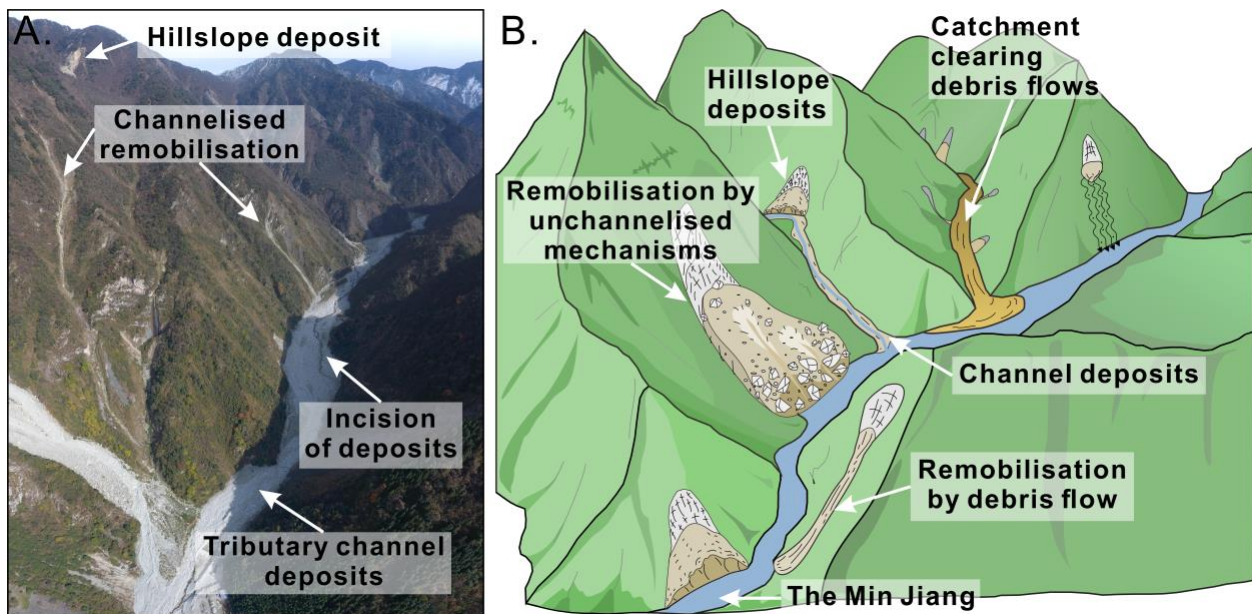176 a sediment budget is important to determine the likely future of the area.
177
178

180 **Figure 2. A)** Drone image of a subcatchment of the Min Jiang, taken in October 2019. The main
181 sediment storage types are highlighted as well as the visible signs of sediment transport. B) A
182 conceptual cartoon of the Min Jiang following the earthquake. The main sediment transport
183 processes are represented along with their sources and sinks.

184

185 **2 Materials and Methods**

186 2.1 Study area and structure of the sediment budget

187 Our sediment budget covers the reach of the Min Jiang between the towns of Yingxu, close to
188 the epicentre of the earthquake, and Wenchuan town (Figure 1). The study focused on the 28
189 catchments which discharge directly into the main trunk of the Min Jiang (Figure 1B). We
190 mapped the coseismic and postseismic landslides between 2008 and 2018 to estimate the volume
191 of sediment that moved from the hillslope into the Min Jiang during this period. Using the

192 multitemporal inventories we identified the key sediment transfers and stores within our study
193 area.
194
195　　　　2.2 Multitemporal landslide inventory
196
197 The multitemporal landslide inventory is the basis of our sediment budget as it constrains the
198 volume of sediment generated during our study period and the transfer of sediment from the
199 hillslope to the channel network. This inventory is an adapted version of the inventory described
200 in Fan et al. (2019b), here we will briefly describe the methodology used to generate this
201 inventory and the key alterations we made.
202
203 The inventory is derived from orthorectified satellite (and some aerial) imagery of 6 different
204 years after the earthquake (Table S1). The 2011 image provided coverage of the entire area in
205 high resolution and hence was chosen as the geo-referencing base for the study. Each image was
206 orthorectified using the Pix4D software before detailed checks were employed to ensure there
207 were no major rectifying errors between the inventories (Williams et al. 2018). In each image we
208 visually mapped any new mass movements along with any remobilisation within the mass
209 movements mapped in a previous image. Mass movements were mapped as polygons which
210 covered the entire area of the mass movement, no effort was made to separate the source and
211 deposition areas. New mass movements were identified by the stripping of vegetation from the
212 hillslope which do not intersect with any previous mass movements. Remobilisation was mapped
213 by identifying changes within previously mapped mass movements (Figure S1). These changes
214 could be the formation of rill networks, debris flows or landslide scars, or the clear movement of
215 boulders. Any mass movement which intersected with a previously mapped mass movement was
216 classified as a remobilisation due its final volume likely including entrained previously deposited
217 sediment. This classification system differs from the 'activity level' used in original inventory
218 where landslides are classified by the area of the polygon not covered by vegetation (Tang et al.
219 2016; Fan et al. 2019c). Our mapping scheme allowed us to directly map the area of the
220 remobilisation which we then used as the base of our sediment budget.
221
222 Within this mapping scheme we classified two processes in each epoch; landslides and debris
223 flows using the definitions of Fan et al. (2018) (Figure S1). This classification was determined
224 visually based upon the shape of the mapped polygons. Debris flows polygons are long and thin
225 possibly with visible leeves while landslides are wide with no channelisation visible. We also
226 classified remobilisation using a similar scheme, however as less data exists for these processes,
227 we used more generalised terms. Remobilisation polygons which are long and thin were
228 classified as channelised remobilisation (debris flows). Remobilisation polygons without any
229 clear channelisation were defined as unchannelised, these can be formed by shallow landsliding
230 within a previous deposit or may be produced by a dense, impossible to resolve from the
231 imagery, rill network (Figure 1).
232
233　　　　2.3 Literature review derived processes and volumes
234 Alongside the processes identified in the multitemporal landslide inventory we conducted a
235 review of the post Wenchuan earthquake literature to identify other processes which are taking
236 place in the area. These are described below:

237

238 **Catchment clearing debris flows** are large debris flows which evacuate volumes of sediment
239 from the hillslope and tributary channels directly into the Min Jiang. The volumes of these
240 processes were quantified from the database of debris flow events collated by Fan et al. (2019b).
241 This database consists of any large debris flow event recorded in technical reports or papers,
242 most of which had reported volumes of the deposition fan of the event. As uncertainty data was
243 unavailable for most of the events, we assumed ± 50% of the reported volume. The volume of
244 the debris flow was assumed include an even mixture of hillslope and tributary channel deposit
245 material.
246 **Overland flow erosion of mass movements** is an estimate of the volume of sediment removed
247 from bare sediment by runoff. We estimated the volume removed by this process using the field
248 measurements performed by Fusun et al (2013). They deployed sediment traps to record the
249 volume of sediment leaving landslides over a monsoon period and reported their results in the
250 form g/m^2. We used these results and extrapolated them, assuming a constant erosion rate, across
251 the active bare area of the mass movements for each time step. Uncertainty was calculated using
252 a range of bulk densities for the coseismically generated sediment as well as the range of field
253 recorded erosion rates.
254 **Suspended sediment** is also included in our budget as a separate process as it is one of the only
255 records of sediment transport and erosion in the channel network. The suspended sediment
256 discharge is calculated from the measurements reported by Wang et al. (2015). Using daily
257 records of suspended sediment concentration and water discharge Wang et al. (2015) calculated
258 the increase in sediment transported by the rivers draining the orogen after the earthquake. We
259 assumed the increase in sediment discharge was related to the volume of sediment upstream of
260 the recording station and thus scaled the increase by the volume of sediment in our study area.
261 We kept the discharge constant throughout time as the processes behind the timescale of the
262 enhancement are unknown. Uncertainty in our values is as reported in Wang et al. (2015).
263

264 **3 Constructing the sediment budget**

265   3.1 Volume estimates of coseismic and post seismic landslides

266 The mapped area of coseismic landslides is commonly converted into an estimated volume using
267 the empirical area-volume scaling relationship ($V = \alpha A^Y$ where *V* is the volume of the landslide,
268 *A* is its mapped area and α and *Y* are empirical parameters). As the volume of only a small
269 number of landslides has ever been measured these scaling parameters have significant
270 uncertainty (Larsen et al. 2010; Li et al. 2014). Due to this uncertainty, and the small number of
271 landslide volume measurements in the Wenchuan epicentral area, we use the methodology
272 proposed by Li et al. (2014) to calculate the volume of our mapped co- and post-seismic
273 landslides. This method uses a Monte Carlo simulation of six sets of scaling parameters to
274 estimate the total landsliding volume of an epoch and its uncertainty. Each simulation uses a
275 randomly chosen α and *Y* values for each polygon from a normal distribution limited by the
276 uncertainty stated in table 1. We ran 50,000 Monte Carlo simulations for each of the scaling
277 relationships and calculated the total landsliding volume for each simulation. We then calculated
278 the median, 16th and 84th quartiles of the simulations to determine the total landsliding volume
279 and its uncertainty. The combined volume estimate is derived from a dataset of all the results of
280 the simulations of the scaling relationships.

281

Reference	Log$_{10}\alpha$	Y	Total Coseismic Volume (km^3)	Total Post Seismic Volume (km^3)
(Larsen et al. 2010)	-0.836 ±0.015	1.332 ±0.005	6 ×10-1 (±1×10^{-3})	3×10^{-3} (± 3×10^{-5})
(Larsen et al. 2010)	-0.73 ±0.06	1.35 ±0.01	1 (±1×10^{-3})	4×10^{-3} (±1×10^{-4})
(Larsen et al. 2010)	-0.59 ±0.03	1.36 ±0.01	1 (±7×10^{-3})	7×10^{-3} (±1×10^{-4})
(Guzzetti et al. 2009)	-1.131	1.45 ±0.009	1 (±4×10^{-3})	4×10^{-3} (±7×10^{-5})
(Parker et al. 2011)	-0.974 ±0.366	1.388 ±0.087	2 (±1×10^{-1})	6×10^{-3} (-1/+2×10^{-3})
(Li et al. 2014)	-0.995 ±0.366	1.392 ±0.087	2 (±1×10^{-1})	6×10^{-3} (-1/+2×10^{-3})
Combined			1 (-6/+5×10^{-1})	5×10^{-3} (±2×10^{-3})

282 **Table 1.** The results of the Monte Carlo Simulations. Each set of parameters is run 50,000 times
283 and combined to produce an overall estimate of total volume and uncertainty. Coseismic volume
284 includes all landslides that are mapped in the 2008 image while the post-seismic volume includes
285 all new landslides mapped after this year.

286 3.2 Estimating the volume of tributary channel deposits

287 In order to constrain the volume of sediment entering the channel between each image we first
288 produced an independent estimate of the sediment stored. This estimate is then compared to the
289 estimates of sediment transfer produced by the sediment budget in order to identify and dismiss
290 inappropriate area – volume scaling parameters. If a set of parameters produces an estimate of
291 sediment transfer from the hillslope to the channel network significantly outside of the range
292 produced by the independent estimate it is removed from consideration (Table S2).

293

294 This independent budget of the tributary channel deposits was constructed by mapping the cross-
295 sectional width of the active channel deposits in the tributary catchments. The cross-sectional
296 width was defined as the border of sediment from one side of the channel to the other (Figure
297 S2). This width was then mapped at regular intervals for each catchment in each epoch. During
298 times of deposition these widths would increase while during times of low sediment input, they
299 would remain relatively stable.

300

301 To estimate the volume of the channel deposits we simply assumed a triangular cross-sectional
302 area and interpolated across the distance between the cross-section locations. Each time an
303 increase in width was recorded we assumed a corresponding increase in the depth of the deposit
304 and subtracted the previous volume to estimate the change in stored volume over the epoch
305 (Figure S3). As we were unable to map the angle of the base of catchment hillslopes, we used
306 slope angles of 20 and 40 to determine the cross-sectional area. Therefore, the minimum estimate
307 assumes a deposit side angle of 20 degrees while the maximum assumes an angle of 40 for each
308 cross section.

309
310 During times of minimal deposition, we estimated the volume of sediment that is removed from
311 the channel deposits by reworking by the channel. For this we simply measured the width of the
312 actively incising channel and again assumed a triangular cross section. For the bank angles of the
313 channel we used the angle of repose of landslide deposits estimated by Wang et al. (2013). As
314 debris flows are also active in the tributary channel deposits and we could not separate the effects
315 of these and fluvial erosion we term this erosion incision.

316   3.3 Transfer of sediment between hillslope and channels

317 While there are several empirical area – volume scaling relationships for landslides it is unclear
318 whether they are suitable for use with debris flows and remobilisations (Marc and Hovius 2015).
319 To determine the volume of sediment entering the channel deposits we tested a variety of scaling
320 equations using the Monte Carlo method described earlier and compared them to our
321 independent estimate of channel deposit volume (Table S2). Any scaling relationships which
322 produce total volume estimates outside of the independent range are removed from the Monte
323 Carlo simulations.
324
325 To determine whether a mass movement transfers sediment into the tributary channel deposits
326 we compared the maximum drainage area of the mapped polygon with a hillslope/channel
327 threshold. This threshold was derived from a threshold based channel extraction algorithm in the
328 software LSDTopoTools (Mudd et al. 2020). An initial estimate of a threshold was derived from
329 mapping likely channel head locations in satellite imagery. However due to the uncertainty in
330 this approach we created a new threshold from the extracted channel network by determining the
331 median drainage area of a first order channel. If a remobilisation shapefile had a drainage area
332 greater than this threshold it is assigned to the tributary channel deposits. We also calculated the
333 median drainage area of larger order streams in order to determine whether sediment was
334 deposited directly into the Min Jiang.
335
336 Using this methodology, we concluded that remobilisation shapefiles and new mass movement
337 shapefiles need separate area – volume scalings. The landslide area-volume scaling relationships
338 used previously (Table 1) considerably overestimate the volume of sediment mobilised and were
339 therefore excluded from consideration (Table S2). Instead we used a combination of the shallow
340 soil landslide scaling derived by Larsen et al. (2010) ($Log_{10}\alpha$ = -0.836 ±0.015, Y = 1.145
341 ±0.008) and average depths between 0.05 and 0.95m.

342   3.4 Sources and stores

343 To finalise our budget we must identify the sources and stores of each identified process. A key
344 observation of our multitemporal landslide inventory is that the channel network does minimal
345 erosion to landslide deposits which were not directly deposited into the Min Jiang. Minimal
346 undercutting of landslide deposits was observed in the field and satellite imagery suggesting that
347 hillslope processes are the main way by which landslides are eroded. The tributary channels are
348 small and do not have the transport capacity to mobilise the coarse sediment of the deposits.
349 Therefore in our sediment budget all landslides are initially added to the hillslope deposit store
350 unless they are deposited directly into the Min Jiang. Debris flows by contrast can deposit
351 directly into the tributary channel deposits (or the Min Jiang) as their mobility is great enough
352 allows them to travel along the channel before depositing.

353
354 All remobilisation processes from the hillslope can deposit in any store depending on the
355 mobility of the mass movement and the original location of the source sediment. Catchment
356 clearing debris flows can be triggered by remobilisation from the hillslope, run off with in the
357 channel, or the merging of multiple debris flows (Tang et al. 2012; Cui et al. 2013). Due to the
358 complexity in triggering we simply assume the final volume of the deposit comes equally from
359 the hillslope and the tributary channels.

4 Results

360

4.1 Full post-earthquake sediment budget

361

362 In the study area, we mapped a total of 15,130 mass movements (8,830 coseismic and 6,300 post
363 seismic) across the study period (Fig 1B). These mass movements generated a total volume of
364 1.1 (±0.5) km^3 of sediment. 96% of the sediment was generated coseismically, indicating any
365 post seismic enhancement of landsliding is not a significant contributor to post seismic sediment
366 discharges. Of the sediment that was mobilised from the hillslope after the earthquake, less than
367 1% was from new post seismic mass movements suggesting the increase in sediment discharge
368 records is almost exclusively driven by remobilisation of coseismic sediment. Nearly half of the
369 sediment deposited into the Min Jiang, 48.1% (1.9×10^{-2} -8.5/+7.6×10^{-3} km^3), was from coseismic
370 landslide material deposited directly into the river (Table 2). The majority of sediment deposited
371 into the Min Jiang after the earthquake came from the tributary channel deposits. Just 8.1%
372 (1.6×10^{-3} -3×10^{-4}/+6.9×10^{-3} km^3) of the sediment postseismically deposited into the Min Jiang
373 was done so directly from hillslope deposits. Therefore the sediment cascade is the primary way
374 by which sediment is evacuated from the orogen.

375
376 At the end of the decade long study, we found that 93.8% (-6.2+0.3%) of the sediment generated
377 during and after the earthquake remains on the hillslope. 2.8% (-0.8/+6%) is found in the
378 tributary channel deposits and the final 3.4% (+0.5%) has been deposited into the Min Jiang
379 (Figure 3). Of the sediment that was deposited on the hillslope during the earthquake 95.7%
380 remains. 85.4% (4×10^{-2} -2.2×10^{-2}/+1.1×10^{-1} km^3) of the sediment is remobilised from the
381 hillslope is deposited into the tributary channel deposits where it requires further remobilisation
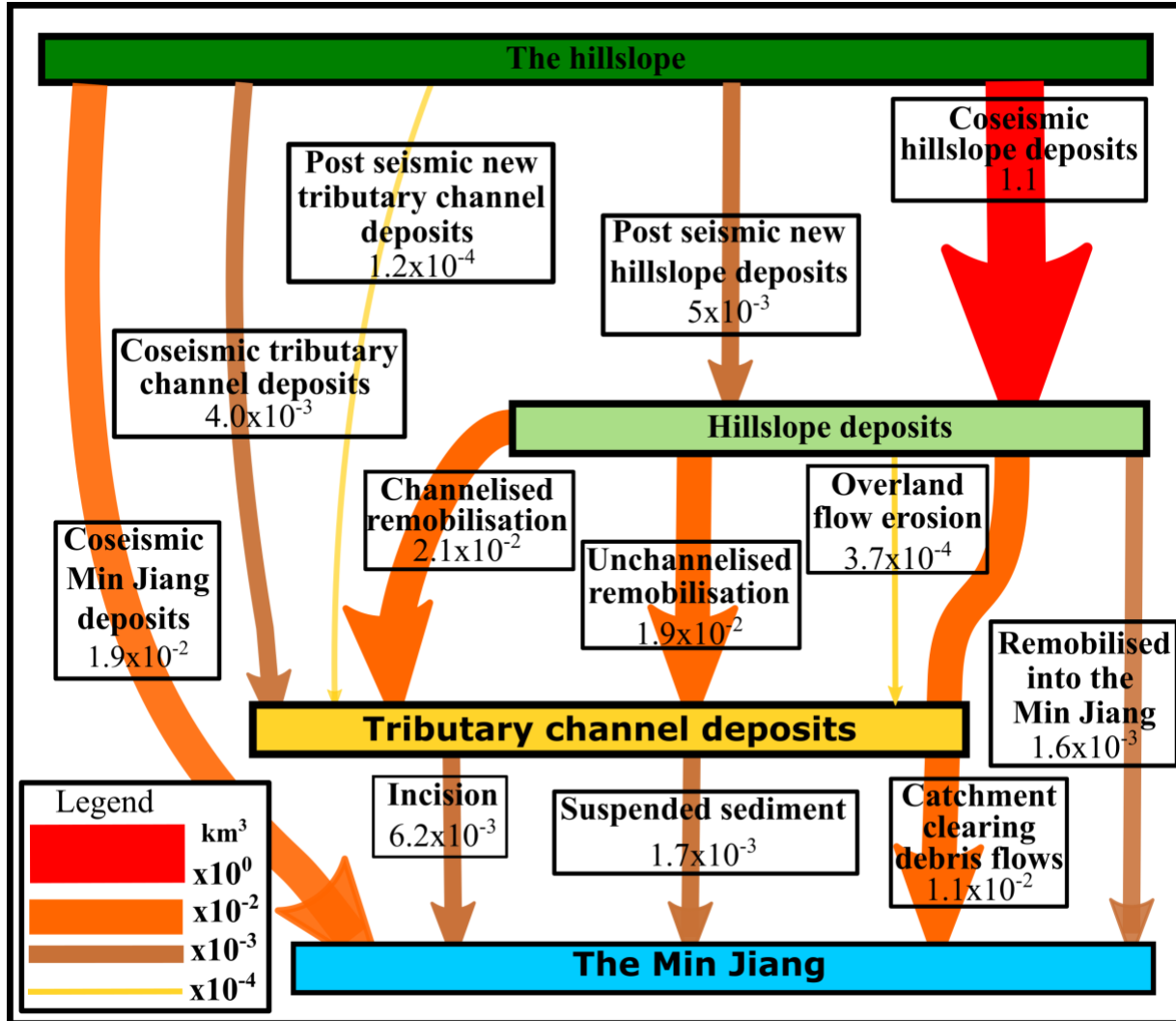382 before it is evacuated from the orogen.
383

384
385

Figure 3. The sediment budget of the Wenchuan Earthquake. The width and colour of each arrow indicates the magnitude of the sediment moved by the process between the stores. Catchment clearing debris flows erode sediment from both hillslope and tributary channel deposits and is represented by an arrow passing through the tributary channel deposits in a single motion. The budget is also shown in table form in Table 2.

Large catchment clearing debris flows are the major process depositing sediment into the Min Jiang accounting for 52.4% ($1.1 \times 10^{-2} \pm 5.2 \times 10^{-3}$ km^3) of the sediment deposited into the river after the earthquake. Debris flows (both small channelised remobilisations and large catchment clearing flows) dominate the sediment budget accounting for 50% (3.3×10^{-2} $-1.6/+7.5 \times 10^{-2}$ km^3) of all sediment mobilised. Fluvial processes (here represented by incision and suspended sediment), on the other hand, are only minor contributors to sediment transport over our study period.

400

401
402

Coseismic sediment budget	Volume (km^3)	Uncertainty (km^3)	%
Coseismic hillslope deposits	1.1	± 0.53	97.5
Coseismic tributary channel deposits	4.0×10^{-3}	$-1.8\times10^{-3}/+1.4\times10^{-2}$	0.4
Coseismic Min Jiang deposits	1.9×10^{-2}	$-8.5/+7.6\times10^{-3}$	1.6
Post-seismic new landslides and debris flows			
Post seismic new hillslope deposits	5.0×10^{-3}	$-1.8/+4.2\times10^{-3}$	0.4
Post seismic new tributary channel deposits	1.2×10^{-4}	$-2.2\times10^{-5}/+7.8\times10^{-4}$	0.0
Total sediment generated	**1.13**	± 0.55	
Remobilisation of hillslope deposits			
Channelised remobilisation	2.1×10^{-2}	$-1/+6.3\times10^{-2}$	1.8
Unchannelised remobilisation	1.9×10^{-2}	$-1.2/+4.4\times10^{-2}$	1.7
Into the Min Jiang	1.6×10^{-3}	$-3\times10^{-4}/+6.9\times10^{-3}$	0.1
Overland flow erosion	3.7×10^{-4}	$\pm7.3\times10^{5}$	0.0
Remobilisation of channel deposits			
Catchment clearing debris flows	1.1×10^{-2}	$\pm5.23\times10^{-3}$	0.9
Suspended sediment	1.7×10^{-3}	$-7\times10^{-4}/+1.2\times10^{-3}$	0.2
Incision	6.2×10^{-3}	$\pm1.01\times10^{-3}$	0.6
Stores			
Hillslope deposits	1.06	$-0.5/+0.4$	93.8
Tributary channel deposits	3.1×10^{-2}	$-2\times10^{-2}/+1.2\times10^{-1}$	2.8
Min Jiang	3.9×10^{-2}	$-1.6/+2.2\times10^{-2}$	3.4

403 **Table 2.** The full sediment budget from figure 3 in table form. All values are rounded to 1
404 significant figure. The percentage values are derived from the median value of each process and
405 the total sediment generated.

406   4.2 The sediment budget through time

407   Using the satellite images we can separate the budget into 4 epochs (2008 – 2011, 2011 – 2013,
408   2013 – 2015, and 2015 – 2018) to analyse how the processes and overall discharge changes
409   through time. We find that the average total discharge (the sum of all processes) decreases by an
410   order of magnitude from 1.4×10^{-2} ($-7.8\times10^{-3}/+2.7\times10^{-2}$) – 1×10^{-3} ($-2.7\times10^{-4}/+7.5\times10^{-4}$) km^3/year
411   (Table 3). A total of 6.4×10^{-2} ($-3.1\times10^{-2}/+1.3\times10^{-1}$) km^3 of sediment (both new and remobilised
412   coseismically generated) is mobilised after the earthquake, 90.8% of which was mobilised during
413   the first 5 years after the earthquake. The total sediment discharge decreases rapidly until 2015
414   after which it begins to level off suggesting it had begun to stabilise by the end of the study
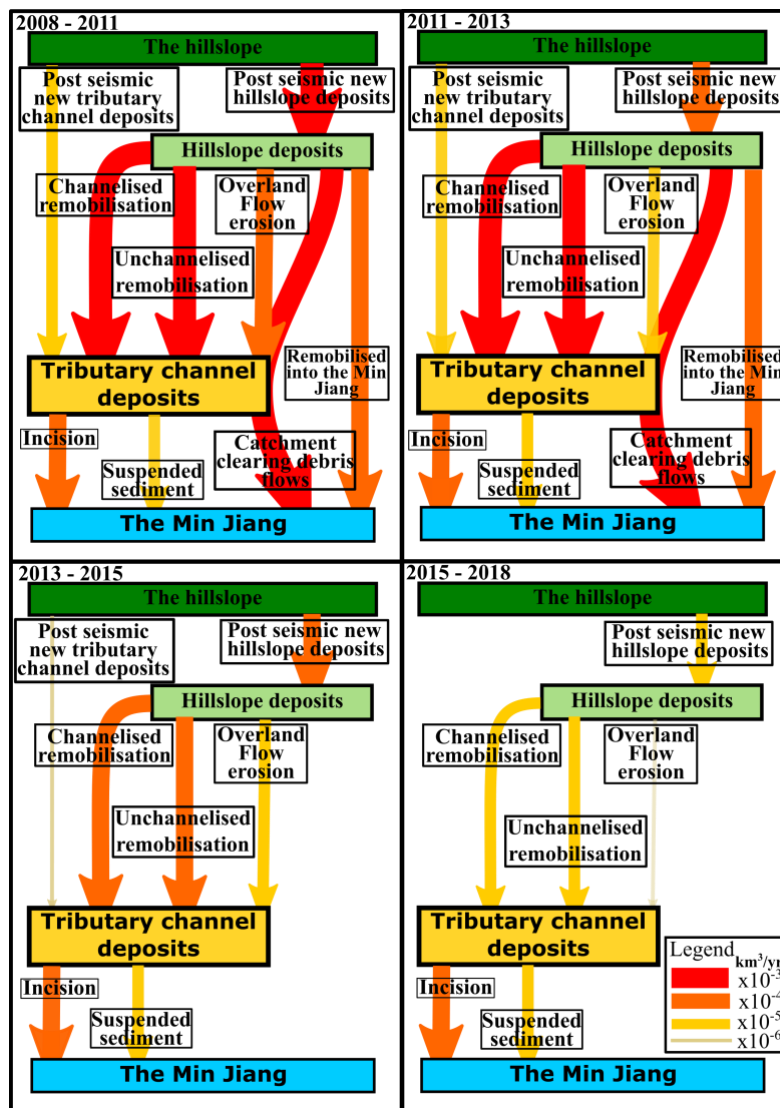415   period.

416

417
418   **Figure 4.** The sediment budget separated into the 4 postseismic epochs. Numbers in the store
419   labels describe the average yearly sediment budget for that store (km^3/yr). The thickness of the
420   arow reflects the magnitude of the sediment transfer while the colour represents the source of the
421   sediment. If a transfer path becomes inactive during a particular epoch the arrow is removed
422   from the diagram.

423
424   The rate at which the hillslope deposits are depleted decreases by 3 orders of magnitude from
425   1.1×10^{-2} (-6.4×10^{-3}/$+2.54\times10^{-2}$) – 4.7×10^{-5} (-2.9×10^{-5}/$+5\times10^{-4}$) km^3/year over our study period.
426   For each epoch the volume of sediment produced by postseismic mass movements (new
427   landsliding and debris flows) is less than the volume remobilised from the hillslope deposits.
428   This decrease in remobilisation rates coincides with the overall decrease in sediment discharge.
429   As remobilisation of coseismic deposits continues to dominate the hillslope sediment discharge
430   at the end of our study period, it is likely the overall discharge remains elevated above pre-
431   earthquake levels.
432
433   Tributary channels have aggraded due to the high volumes of sediment deposited into them.
434   Only after 2013 do the tributary channel deposits erode rather than aggrade. This is despite the
435   major eroding process of the tributary channel deposits, the catchment clearing debris flows,
436   ceasing to occur within our study area. The major cause of the negative tributary channel deposit
437   budget seems to be due to a decrease in the volume of sediment being deposited within the
438   channels. A slight increase in the volume of sediment leaving the deposits via incision is seen,
439   however due to a lack of constraints we are not able to verify this pattern. If the deposition of
440   sediment into the tributary channel deposits remains low it is likely the total volume of sediment
441   stored will continue to decrease.
442
443   Finally, we see an overall decrease in the volume of sediment entering the Min Jiang due to the
444   ceasing of large catchment clearing debris flows. Without these large flows the volume of
445   sediment entering the Min Jiang decreases by an order of magnitude, highlighting the importance
446   of the largest events to evacuating the coseismic sediment from the Longmen Shan.
447
448

449

All units km³/yr	2008 -2011	2011-2013	2013-2015	2015 - 2018
Post-seismic new landslides and debris flows				
Post seismic new hillslope deposits	1.1×10^{-3} $(-4/9\times10^{-4})$	6.4×10^{-4} $(-2.3/+5.7\times10^{-4})$	1.4×10^{-4} $(-4.8\times10^{5}/+1.4\times10^{4})$	4×10^{-5} $(-1.3/+2.4\times10^{-5})$
Post seismic new tributary channel deposits	2.6×10^{-5} $(-4.8\times10^{-6}/+1.5\times10^{-4})$	2.1×10^{-5} $(-3.5\times10^{-6}/+1.7\times10^{-4})$	3.6×10^{-6} $(-5.7\times10^{-7}/+2.8\times10^{-5})$	0
Remobilisation of hillslope deposits				
Channelised remobilisation	4.9×10^{-3} $(-2.6\times10^{-3}/+1.3\times10^{-2})$	2.5×10^{-3} $(-1/+9\times10^{-3})$	4.0×10^{-4} $(-8\times10^{-5}/+2.2\times10^{-3})$	2.2×10^{-5} $(-4\times10^{-6}/+1.24\times10^{-4})$
Unchannelised remobilisation	5×10^{-3} $(-3.3\times10^{-3}/+1\times10^{-2})$	1.9×10^{-3} $(-1.1/+5.6\times10^{-3})$	1.3×10^{-4} $(-4.1/6.7\times10^{-4})$	6.2×10^{-5} $(-1.1\times10^{-5}/+3.6\times10^{-4})$
Into the Min Jiang	2.7×10^{-4} $(-5\times10^{-5}/+1.1\times10^{-3})$	4.1×10^{-4} $(-7.5\times10^{-5}/+1.7\times10^{-3})$	0	0
Overland Flow erosion	2.9×10^{-4} $(\pm5.6\times10^{-5})$	5.8×10^{-5} $(\pm1.13\times10^{-5})$	2.2×10^{-5} $(\pm4.3\times10^{-6})$	3.1×10^{-6} $(\pm6\times10^{-7})$
Remobilisation of Channel deposits				
Catchment clearing debris flows	2.5×10^{-3} $(\pm1.3\times10^{-3})$	1.4×10^{-3} $(\pm7.1\times10^{-4})$	0	0
Suspended sediment	5.3×10^{-5} $(\pm2.3\times10^{-5})$	5.3×10^{-5} $(\pm2.3\times10^{-5})$	5.3×10^{-5} $(\pm2.3\times10^{-5})$	5.3×10^{-5} $(\pm2.3\times10^{-5})$
Incision	1.9×10^{-4} $(\pm5\times10^{-5})$	4.9×10^{-4} $(\pm1.3\times10^{-4})$	6.8×10^{-4} $(\pm1.8\times10^{-4})$	8.3×10^{-4} $(\pm2.2\times10^{-4})$

450   **Table 3.** The sediment budget separated into 4 epochs with each process quantified and averaged
451   across the epoch. All units are in km³/yr

452   **5 Discussion**

453   Our full sediment budget of the Wenchuan earthquake reveals that over 90% of the sediment
454   produced by the earthquake remains on the hillslope 10 years after the earthquake. The majority
455   of the coseismically generated sediment is mobilized by debris flows, either small flows which
456   deposit sediment to the base of the hillslope or rare large flows which can bypass the tributary
457   channel deposits and mobilise sediment directly into the Min Jiang. While the largest catchment
458   clearing debris flows are relatively frequent during the first few years after the earthquake it is

459 unlikely they will continue occur as often as this in the future. This suggests that most sediment
460 will have to pass through the tributary channel deposit store before it is mobilised out of the
461 system. This pattern of remobilisation and deposition could be repeated multiple times likely
462 extending the residence time of some sediment up to 100s if not 1000s of years.

464 Our sediment budget also demonstrates that the rate at which sediment is remobilised from the
465 hillslope has decreased since the earthquake. In the first epoch (2008-2011) of our budget we
466 recorded 4296 remobilisation events, 1193 of which were channelised. However, in the final
467 epoch (2015-2018) just 54 remobilisations were recorded (11 channelised). Despite there being
468 more unchannelised remobilisations than channelised, channelised remobilisations more
469 frequently deposited sediment into the channel network due to their longer runouts making them
470 near equal contributors. This rapid reduction in remobilisation frequency is most likely due to a
471 stabilisation of the hillslope deposits rather than exhaustion due to the large volume of sediment
472 remaining on the hillslope. This apparent stabilisation of the hillslope deposits will also extend
473 the residence time of coseismically generated sediment beyond that of what can be expected
474 from rates recorded here. The reduction in debris flow frequency we observe is also reported in
475 other studies; rainfall intensity duration thresholds in the epicentral area have increased since the
476 earthquake leading to indications of a stabilisation of the coseismically generated sediment
477 taking place (Zhang and Zhang 2017; Fan et al. 2020).

479 The mechanisms behind this apparent stabilisation are still unknown, however there are several
480 theories which we will discuss here. The first is that colonisation of the landslide area by
481 vegetation has increased the resistive strength of the landslide deposit. Depending on the
482 triggering mechanism of the failure vegetation can stabilise the deposit in several ways. The
483 canopy of vegetation can intercept the rainfall before it strikes the sediment reducing the local
484 intensity and saturation state (Wilkinson et al. 2002; McGuire et al. 2016). While the trunks and
485 stems of vegetation increase the roughness of the slope reducing the speed of any potential
486 surface runoff reducing the stress applied to the sediment. Vegetation can suck water out and
487 increase the shear strength of the soil increasing the intensity required to produce failure through
488 saturation (Hales et al. 2009; Hales 2018). Vegetation is seem as a contender to stabilising the
489 coseismically generated sediment due to satellite observations which show that NDVI
490 (Normalised Difference Vegetation Index) values are returning rapidly to pre-earthquake levels
491 (Shen et al. 2020; Yunus et al. 2020). This rebound in vegetated area appears to be well
492 correlated with a reduction in remobilisation of sediment (Fan et al. 2018; Yunus et al. 2020).
493 However the first vegetation to colonise the landslide areas tend to be grasses and shrubs (Shen
494 et al. 2020), most of which only have shallow and weak root structures which do not add
495 significant strength to the sediment (Hales 2018). Therefore if saturation is the main way by
496 which debris flows and landslides occur within the coseismically generated sediment it is
497 unlikely vegetation is the main mechanism by which the sediment is stabilised. If instead surface
498 runoff is the main way by which sediment is remobilised it is possible grasses and shrubs may
499 slow runoff enough to prevent debris flows from occurring. However it is currently unclear how
500 remobilisation is triggered in hillslope deposits but it is unlikely vegetation is the only
501 mechanism by which sediment is stabilised.

503 The other mechanism which has been proposed to explain the stabilisation of the hillslope
504 deposits is internal erosion which preferentially removes fine sediment from the deposits (Cui et

505 al. 2014; Hu et al. 2016; Hu et al. 2017; Zhang and Zhang 2017). It is hypothesised that fresh
506 landslide deposits are highly permeable which allows water to pass through easily. As the water
507 passes through the deposit it can entrain the fine sediment and transport it out of the deposit. This
508 muddy mixture can then induce localised failures within the deposit in less permeable parts of
509 the deposit (Cui et al. 2014). If enough of these small failures occur it is possible a debris flow
510 can be formed. However if no large scale failure occurs the deposit will be left in a fines depleted
511 state which is more porous and permeable and as a result less favourable for failure in the future
512 (Hu et al. 2016; Hu et al. 2017). The smaller failures may also compact the deposits which has
513 also been shown to reduce the likelihood of failure in loose sediment (Iverson et al. 2000; Gabet
514 and Mudd 2006; Chang et al. 2011). However, there is minimal in situ evidence for this theory of
515 preferential erosion of fine sediment. The primary source of field evidence for this coarsening is
516 from debris flow deposit sequences (Chen et al. 2014; Zhang et al. 2014; Yang et al. 2021). The
517 newer debris flow deposits are significantly coarser than the older deposits, however it is not
518 clear whether the patterns in the deposit reflect the processes occurring in the source. Finally, for
519 this coarsening process to be a significant factor in the stabilisation of hillslope deposits across
520 the area it is likely vast volumes of fine sediment would have to be mobilized and deposited into
521 the Min Jiang. However, the suspended sediment discharge of the river returned to pre-
522 earthquake levels before significant volumes of sediment could be mobilised (Wang et al. 2015).
523
524 Small debris flows are the major process in remobilising sediment from the hillslope into the
525 tributary channel deposits while large catchment clearing debris flows are the main process by
526 which sediment is deposited into the Min Jiang. After 2013 there are no large catchment clearing
527 debris flows and as a result the volume of sediment entering the Min Jiang decreases by an order
528 of magnitude. In contrast the fluvial driven processes (termed incision in our budget) are much
529 more stable but significantly less important. Incision only accounts for 15% of the sediment
530 deposited into the Min Jiang during the first decade after the earthquake. Fluvial erosion is only
531 observed acting on sediment that has already been remobilised once, there is little evidence that
532 the tributary channels can erode the landslide deposits directly. This further highlights the
533 importance of hillslope processes in remobilising sediment prior to it being available for
534 evacuation from the orogen. Fluvial erosion is likely slow at removing sediment from the
535 tributary channel deposits due to the coarse nature of the stored sediment. Cobble and boulder
536 sized grains are not uncommon and require significantly larger than average discharges to
537 mobilise them. The coarse nature of the tributary channel deposits indicates that much of the
538 sediment requires debris flows, large floods or in situ break down of the boulders before it can be
539 mobilised out of the orogen.
540
541 It is important to point out that we have little to no constraints on the volume of sediment that
542 leaves the tributary channel deposits unless it is by a catchment clearing debris flow. Without
543 these constraints we have to assume that the volume of sediment that is entrained by our incision
544 term is immediately removed from the tributary channel deposits. As most sediment will be
545 deposited before it exits the tributary channel deposits it is possible our estimation of the
546 sediment volume transported into the Min Jiang is an over estimation. Therefore we can be
547 confident in stating that incision is a minor contributor to the sediment budget. Improving our
548 estimation of the volume of sediment entering the Min Jiang via fluvial processes will require
549 monitoring of both water and sediment discharge of the tributary catchments.
550

551 Finally, it is unlikely the incision mapped as part of the study is exclusively derived by fluvial
552 processes. Debris flows are common on the tributary channel floors and these can mobilise
553 sediment and create channels which may not separable from fluvially derived channels. It has
554 also been suggested that debris flow activity in the tributary channel deposits could become more
555 common through time as more aggradation occurs (Zhang and Zhang 2017; Fan et al. 2018). We
556 observe a slight increase in the incision term in the final epochs of our sediment budget. If this
557 increase is real and represents an increase in the volume of sediment entering the Min Jiang it is
558 possible debris flow activity could contribute to this. If this increase in debris flow activity is an
559 indicator of a potential increase in the frequency of large catchment clearing debris flows the
560 tributary channel deposits could be evacuated rapidly during times of high sediment availability.
561 However, without a clear understanding of the triggering mechanisms of the large catchment
562 clearing debris flows it is not possible to determine a long-term rate by which sediment is
563 exported from these deposits.
564
565 In August 2019 a large storm triggered 12 large catchment clearing debris flows in our study
566 area, some in catchments where no debris flow had occurred for over 5 years (Fan et al. 2020;
567 Yang et al. 2021). These events demonstrate the stochastic nature of the largest but most
568 important events in mobilising sediment through the mountain range. Initial estimates of the
569 volume of the debris flows suggests a total of 1.9×10^{-2} ($\pm3\times10^{-2}$) km^3 of sediment was
570 transported by these events (Yang et al. 2021). However most of this volume was re-deposited
571 within the tributary channel deposits. As a crude estimate of the volume of sediment deposited
572 into the Min Jiang, we can extrapolate the recorded volume of a single debris flow fan over all of
573 the 12 flows. The deposition fan of the Manianping catchment has an estimated volume of 7×10^{-4}
574 km^3 (Yang et al. 2021) assuming all 12 flows were of equal magnitude, 8.4×10^{-3} km^3 of sediment
575 was deposited into the Min Jiang. Including these flows into the final epoch of the step budget
576 would increase the volume of sediment entering into the Min Jiang by an order of magnitude and
577 return the sediment budget to magnitudes not seen since 2013. Interestingly many of the 2019
578 catchment clearing debris flows occurred without significant remobilisation of hillslope deposits,
579 indicating they removed sediment only from the tributary channel deposits (Fan et al. 2020). If it
580 is possible these flows could have evacuated over 20% of the sediment in the tributary channel
581 deposits. These flows demonstrate the need for long-term (multi-decadal) observational records
582 before predictions of future behaviour of post seismic landscapes can be made.
583
584 The Min Jiang drains into the Zipingpu reservoir a few kilometres after leaving the study area
585 providing an excellent opportunity to identify whether the sediment dynamics discussed here can
586 be identified downstream. A borehole of the centre of the reservoir drilled by Zhang et al.
587 (2019) in 2016 identified that the earthquake had only had a slight impact on the sediment
588 dynamics. No change in sedimentation rate was noticed, likely due to the distal location of the
589 core relative to the Min Jiang entering the reservoir, but a change in the chemistry and grain size
590 was observed (Zhang et al. 2019). Grain size increased, possibly indicating the transport of
591 coarser coseismic landslide derived sediment, and the Rb/Sr ratio decreased potentially due to an
592 influx of unweathered (fresh landslide derived) sediment into the reservoir. Crucially while these
593 signals were recognised immediately after the earthquake the biggest response was observed
594 after the 2010 debris flows where significant volumes of coseismically generated sediment was
595 deposited into the rivers draining into the reservoir. This result agrees with our finding that
596 debris flows are the major component in delivering sediment to the channel network. The

597 borehole also suggests that the system is in a transport limited state as grain size and total runoff
598 is well correlated indicating the need for large events to mobilise much of the sediment (Zhang et
599 al. 2019).
600
601 Our and the results of others (West et al. 2014; Wang et al. 2017; Zhang and Zhang 2017; Zhang
602 et al. 2019) indicate that much of the coseismically generated sediment is transport limited. It is
603 either waiting on the hillslope to be remobilised by mass movements or in tributary channel
604 deposits waiting for a flood or large debris flow. This could result in sediment residence times of
605 1000's of years which is likely to impact the long-term evolution of the landscape. Empirical and
606 modelling studies suggest that the hillslope will continue to be perturbed for at least another
607 decade before returning to background levels (Chen et al. 2020; Li et al. 2020; Shen et al. 2020;
608 Yunus et al. 2020). As this trend in declining activity is driven by stabilisation rather than
609 exhaustion it is likely the residence time of the coseismically generated sediment will be
610 significantly longer. Large earthquakes such as the Wenchuan earthquake have a return period of
611 500 – 4000 years and if coseismically generated sediment can remain being reworked for similar
612 timescales it is likely erosion rates will be altered (Li et al. 2017; Francis et al. 2020). The large
613 volumes of sediment on the hillslopes, which are on average steeper than the likely friction angle
614 of sediment, will continue to be mobilised, albeit much slower than immediately after the
615 earthquake. Erosion rates in the tributary channels and the Min Jiang are likely to be lowered if
616 the bedload is not mobilised at rates significant enough to abrade the bed. Deposits of landslide
617 derived sediment have been linked to knickpoints within the Longmen Shan indicating the region
618 is prone to long periods of reduced erosion (Ouimet et al. 2007; Fan et al. 2019a). If post seismic
619 reduction of erosion rates is frequent and wide spread, it is possible that the largest earthquakes
620 may have a positive impact on the long-term mass balance of the mountain range despite the
621 huge amount of erosion they initiate.

6 Conclusions

623 Here we have quantified the sediment cascade of the 10 years following the 2008 Wenchuan
624 earthquake. Using a multitemporal landslide inventory and constrained area – volume scaling
625 relationships we tracked the evolution of 1.1 (±0.5) km^3 of sediment. Of this sediment just 3%
626 was deposited into the Min Jiang, the major orogen draining river of the study area. 95% of the
627 sediment deposited onto the hillslope during the earthquake remains there waiting to be
628 mobilised into the channel network. The key process in mobilising coseismic sediment into the
629 Min Jiang has been debris flows. The largest of these can deposit huge volumes of sediment
630 from the tributary channels, overcoming the otherwise low transport capacity of the channels in
631 these catchments. These large flows are highly stochastic and can occur after breaks of many
632 years. Determining the frequency and magnitude of these events is crucial to estimating the
633 residence time of the coseismically generated sediment. Finally, as large volumes of
634 coseismically generated sediment can remain within the orogen for extended periods of time,
635 their impact should be considered when modelling the long-term evolution of tectonically active
636 mountain ranges.

Acknowledgments, Samples, and Data

References

Bennett, G.L. et al. 2014. A probabilistic sediment cascade model of sediment transfer in the Illgraben. *Water Resources Research* 50(2), pp. 1225–1244. Available at: http://doi.wiley.com/10.1002/2013WR013806.

Burchfiel, B.C. et al. 2008. A geological and geophysical context for the Wenchuan earthquake of 12 May 2008, Sichuan, People's Republic of China. *GSA Today* 18(7), pp. 4–11. doi: 10.1130/GSATG18A.1.

Campforts, B. et al. 2020. HyLands 1.0: A hybrid landscape evolution model to simulate the impact of landslides and landslide-derived sediment on landscape evolution. *Geoscientific Model Development* 13(9), pp. 3863–3886. doi: 10.5194/gmd-13-3863-2020.

Chang, D.S. et al. 2011. Field testing of erodibility of two landslide dams triggered by the 12 May Wenchuan earthquake. *Landslides* 8(October 2009), pp. 321–332. doi: 10.1007/s10346-011-0256-x.

Chen, H.X. et al. 2014. Evolution of debris flow properties and physical interactions in debris-flow mixtures in the Wenchuan earthquake zone. *Engineering Geology* 182(PB), pp. 136–147. Available at: http://dx.doi.org/10.1016/j.enggeo.2014.08.004.

Chen, M. et al. 2020. The long-term evolution of landslide activity near the epicentral area of the 2008 Wenchuan earthquake in China. *Geomorphology* 367, p. 107317. doi: 10.1016/j.geomorph.2020.107317.

Croissant, T. et al. 2019. Seismic cycles, earthquakes, landslides and sediment fluxes: Linking tectonics to surface processes using a reduced-complexity model. *Geomorphology* 339, pp. 87–103. doi: 10.1016/j.geomorph.2019.04.017.

Cui, P. et al. 2013. Scale amplification of natural debris flows caused by cascading landslide dam failures. *Geomorphology* 182(August 2010), pp. 173–189. doi: 10.1016/j.geomorph.2012.11.009.

Cui, P. et al. 2014. The mechanisms behind shallow failures in slopes comprised of landslide deposits. *Engineering Geology* 180, pp. 34–44. Available at: http://dx.doi.org/10.1016/j.enggeo.2014.04.009.

Dadson, S.J. et al. 2004. Earthquake-triggered increase in sediment delivery from an active mountain belt. *Geology* 32(8), p. 733. Available at: https://pubs.geoscienceworld.org/geology/article/32/8/733-736/29559.

Dahlquist, M.P. et al. 2018. Landslide-driven drainage divide migration. *Geology* 46(5), pp. 403–406. doi: https://doi.org/10.1130/G39916.1.

Dai, F.C. et al. 2011. Spatial distribution of landslides triggered by the 2008 Ms 8.0 Wenchuan earthquake, China. *Journal of Asian Earth Sciences* 40(4), pp. 883–895. doi: 10.1016/j.jseaes.2010.04.010.

Densmore, A.L. et al. 2007. Active tectonics of the Beichuan and Pengguan faults at the eastern margin of the Tibetan Plateau. *Tectonics* 26(4), pp. 1–17. doi: 10.1029/2006TC001987.

Densmore, A.L. et al. 2010. The role of late quaternary upper-crustal faults in the 12 may 2008 Wenchuan earthquake. *Bulletin of the Seismological Society of America* 100(5 B), pp. 2700–2712. doi: 10.1785/0120090294.

Densmore, A.L. et al. 2012. Reply to 'Isostasy can't be ignored'. *Nature Geoscience* 5(2), pp. 83–84. Available at: http://dx.doi.org/10.1038/ngeo1385.

Egholm, D.L. et al. 2013. Lifespan of mountain ranges scaled by feedbacks between landsliding and erosion by rivers. *Nature* 498(7455), pp. 475–478. doi: 10.1038/nature12218.

Fan, X. et al. 2018. Spatio-temporal evolution of mass wasting after the 2008 Mw 7 . 9 Wenchuan Earthquake revealed by a detailed multi-temporal inventory. *Landslides* 15(September), pp. 2325–2341. doi: 10.1007/s10346-018-1054-5.

Fan, X. et al. 2019a. Comment on 'Gigantic rockslides induced by fluvial incision in the Diexi area along the eastern margin of the Tibetan Plateau' by Zhao et al. (2019) Geomorphology 338, 27–42. *Geomorphology* (xxxx), p. 106963. Available at: https://doi.org/10.1016/j.geomorph.2019.106963.

Fan, X. et al. 2019b. Earthquake-Induced Chains of Geologic Hazards: Patterns, Mechanisms, and Impacts. *Reviews of Geophysics* . doi: 10.1029/2018RG000626.

Fan, X. et al. 2019c. Two multi-temporal datasets that track the enhanced landsliding after the 2008 Wenchuan earthquake. *Earth System Science Data* 11(1), pp. 35–55. Available at: https://www.earth-syst-sci-data.net/11/35/2019/.

Fan, X. et al. 2020. Rapidly evolving controls of landslides after a strong earthquake and implications for hazard assessments. *Geophysical Research Letters* 33(0), pp. 2–31. Available at: https://onlinelibrary.wiley.com/doi/10.1029/2020GL090509.

Francis, O.R. et al. 2020. The impact of earthquakes on orogen-scale exhumation. *Earth Surface Dynamics* 8(3), pp. 579–593. Available at: https://esurf.copernicus.org/articles/8/579/2020/.

Fusun, S. et al. 2013. Effects of different types of vegetation recovery on runoff and soil erosion on a Wenchuan earthquake-triggered landslide, China. *Journal of Soil and Water Conservation* 68(2), pp. 138–145. doi: 10.2489/jswc.68.2.138.

Gabet, E.J. and Mudd, S.M. 2006. The mobilization of debris flows from shallow landslides. *Geomorphology* 74(1–4), pp. 207–218. doi: 10.1016/j.geomorph.2005.08.013.

Gallen, S.F. et al. 2015. Coseismic landslides reveal near-surface rock strength in a highrelief, tectonically active setting. *Geology* 43(1), pp. 11–14. doi: 10.1130/G36080.1.

Godard, V. et al. 2010. Spatial distribution of denudation in Eastern Tibet and regressive erosion of plateau margins. *Tectonophysics* 491(1–4), pp. 253–274. Available at: http://dx.doi.org/10.1016/j.tecto.2009.10.026.

Guo, X. et al. 2016. Intensity-duration threshold of rainfall-triggered debris flows in the

Wenchuan Earthquake affected area, China. *Geomorphology* 253, pp. 208–216. doi: 10.1016/j.geomorph.2015.10.009.

Guzzetti, F. et al. 2009. Landslide volumes and landslide mobilization rates in Umbria, central Italy. *Earth and Planetary Science Letters* 279(3–4), pp. 222–229. Available at: http://dx.doi.org/10.1016/j.epsl.2009.01.005.

Hales, T.C. et al. 2009. Topographic and ecologic controls on root reinforcement. *Journal of Geophysical Research: Solid Earth* 114(3), pp. 1–17. doi: 10.1029/2008JF001168.

Hales, T.C. 2018. Modelling biome-scale root reinforcement and slope stability. *Earth Surface Processes and Landforms* 43(10), pp. 2157–2166. doi: 10.1002/esp.4381.

Hovius, N. et al. 2000. Supply and Removal of Sediment in a Landslide-Dominated Mountain Belt: Central Range, Taiwan. *The Journal of Geology* 108(1), pp. 73–89. Available at: http://www.journals.uchicago.edu/doi/10.1086/314387.

Hovius, N. et al. 2011. Prolonged seismically induced erosion and the mass balance of a large earthquake. *Earth and Planetary Science Letters* 304(3–4), pp. 347–355. Available at: http://dx.doi.org/10.1016/j.epsl.2011.02.005.

Hu, W. et al. 2016. Initiation processes for run-off generated debris flows in the Wenchuan earthquake area of China. *Geomorphology* 253, pp. 468–477. doi: 10.1016/j.geomorph.2015.10.024.

Hu, W. et al. 2017. Sensitivity of the initiation and runout of flowslides in loose granular deposits to the content of small particles: An insight from flume tests. *Engineering Geology* 231(July), pp. 34–44. Available at: https://doi.org/10.1016/j.enggeo.2017.10.001.

Huang, R. and Fan, X. 2013. The landslide story. *Nature Geoscience* 6(5), pp. 325–326. Available at: http://dx.doi.org/10.1038/ngeo1806.

Hubbard, J. and Shaw, J.H. 2009. Uplift of the Longmen Shan and Tibetan plateau, and the 2008 Wenchuan (M = 7.9) earthquake. *Nature* 458(7235), pp. 194–197. Available at: http://dx.doi.org/10.1038/nature07837.

Iverson, R.M. et al. 2000. Acute sensitivity of landslide rates to initial soil porosity. *Science* 290(5491), pp. 513–516. doi: 10.1126/science.290.5491.513.

Keefer, D.K. 2002. Investigating landslides caused by earthquakes - A historical review. *Surveys in Geophysics* 23(6), pp. 473–510. doi: 10.1023/A:1021274710840.

Kincey, M.E. et al. 2021. Evolution of coseismic and post-seismic landsliding after the 2015 M w 7.8 Gorkha earthquake, Nepal. *Journal of Geophysical Research: Earth Surface* . doi: 10.1029/2020jf005803.

Kirby, E. and Ouimet, W. 2011. Tectonic geomorphology along the eastern margin of Tibet: insights into the pattern and processes of active deformation adjacent to the Sichuan Basin. *Geological Society, London, Special Publications* 353(1), pp. 165–188. Available at: http://sp.lyellcollection.org/lookup/doi/10.1144/SP353.9.

Koi, T. et al. 2008. Prolonged impact of earthquake-induced landslides on sediment yield in a mountain watershed: The Tanzawa region, Japan. *Geomorphology* 101(4), pp. 692–702. doi: 10.1016/j.geomorph.2008.03.007.

761   Korup, O. 2012. Earth's portfolio of extreme sediment transport events. *Earth-Science Reviews*
762   112(3–4), pp. 115–125. Available at: http://dx.doi.org/10.1016/j.earscirev.2012.02.006.

763   Larsen, I.J. et al. 2010. Landslide erosion controlled by hillslope material. *Nature Geoscience*
764   3(4), pp. 247–251. Available at: http://dx.doi.org/10.1038/ngeo776.

765   Li, C. et al. 2020. Landscape evolution of the Wenchuan earthquake-stricken area in response to
766   future climate change. *Journal of Hydrology* 590, p. 125244. Available at:
767   https://doi.org/10.1016/j.jhydrol.2020.125244.

768   Li, G. et al. 2014. Seismic mountain building: Landslides associated with the 2008 Wenchuan
769   earthquake in the context of a generalized model for earthquake volume balance. *Geochemistry,*
770   *Geophysics, Geosystems* 15(4), pp. 833–844. Available at:
771   http://doi.wiley.com/10.1002/2013GC005067.

772   Li, G. et al. 2016. Connectivity of earthquake-triggered landslides with the fluvial network:
773   Implications for landslide sediment transport after the 2008 Wenchuan earthquake. *Journal of*
774   *Geophysical Research: Earth Surface* 121(4), pp. 703–724. Available at:
775   http://doi.wiley.com/10.1002/2015JF003718.

776   Li, G. et al. 2017. Earthquakes drive focused denudation along a tectonically active mountain
777   front. *Earth and Planetary Science Letters* 472, pp. 253–265. Available at:
778   http://dx.doi.org/10.1016/j.epsl.2017.04.040.

779   Lin, G.-W. et al. 2008. Effects of earthquake and cyclone sequencing on landsliding and fluvial
780   sediment transfer in a mountain catchment. *Earth Surface Processes and Landforms* 33(9), pp.
781   1354–1373. Available at: http://doi.wiley.com/10.1002/esp.1716.

782   Liu-Zeng, J. et al. 2009. Co-seismic ruptures of the 12 May 2008, Ms8.0 Wenchuan earthquake,
783   Sichuan: East-west crustal shortening on oblique, parallel thrusts along the eastern edge of Tibet.
784   *Earth and Planetary Science Letters* 286(3–4), pp. 355–370. Available at:
785   http://dx.doi.org/10.1016/j.epsl.2009.07.017.

786   Malamud, B.D. et al. 2004. Landslides, earthquakes, and erosion. *Earth and Planetary Science*
787   *Letters* 229(1–2), pp. 45–59. doi: 10.1016/j.epsl.2004.10.018.

788   Marc, O. et al. 2015. Transient changes of landslide rates after earthquakes. *Geology* 43(10), pp.
789   883–886. doi: 10.1130/G36961.1.

790   Marc, O. et al. 2016a. A seismologically consistent expression for the total area and volume of
791   earthquake-triggered landsliding. *Journal of Geophysical Research: Earth Surface* 121(4), pp.
792   640–663. Available at: http://doi.wiley.com/10.1002/2015JF003732.

793   Marc, O. et al. 2016b. The mass balance of earthquakes and earthquake sequences. *Geophysical*
794   *Research Letters* 43(8), pp. 3708–3716. doi: 10.1002/2016GL068333.

795   Marc, O. and Hovius, N. 2015. Amalgamation in landslide maps: Effects and automatic
796   detection. *Natural Hazards and Earth System Sciences* 15(4), pp. 723–733. doi: 10.5194/nhess-
797   15-723-2015.

798   McGuire, L.A. et al. 2016. Constraining the relative importance of raindrop- and flow-driven
799   sediment transport mechanisms in postwildfire environments and implications for recovery time
800   scales. *Journal of Geophysical Research: Earth Surface* 121(11), pp. 2211–2237. doi:
801   10.1002/2016JF003867.

Mudd, S.M. et al. 2020. LSDtopotools/LSDTopoTools2: LSDTopoTools2 v0.3. Available at: https://doi.org/10.5281/zenodo.3769703#.X6AA9d3MMXY.mendeley [Accessed: 2 November 2020].

Ouimet, W.B. et al. 2007. The influence of large landslides on river incision in a transient landscape: Eastern margin of the Tibetan Plateau (Sichuan, China). *Bulletin of the Geological Society of America* 119(11–12), pp. 1462–1476. doi: 10.1130/B26136.1.

Ouimet, W.B. et al. 2009. Beyond threshold hillslopes: Channel adjustment to base-level fall in tectonically active mountain ranges. *Geology* 37(7), pp. 579–582. doi: 10.1130/G30013A.1.

Pain, C.F. and Bowler, J.M. 1973. Denudation following the November 1970 earthquake. *Zeitschrift Fur Geomorphologie* 18, pp. 92–104.

Parker, R.N. et al. 2011. Mass wasting triggered by the 2008 Wenchuan earthquake is greater than orogenic growth. *Nature Geoscience* 4(7), pp. 449–452. Available at: http://dx.doi.org/10.1038/ngeo1154.

Pearce, A.J. and Watson, A.J. 1986. Effects of earthquake-induced landslides on sediment budget and transport over a 50-yr period. *Geology* 14, pp. 52–55.

Roback, K. et al. 2018. The size, distribution, and mobility of landslides caused by the 2015 Mw7.8 Gorkha earthquake, Nepal. *Geomorphology* 301, pp. 121–138. Available at: https://doi.org/10.1016/j.geomorph.2017.01.030.

Royden, L.H. et al. 2008. The Geological Evolution of the Tibetan Plateau. *Science* 321(5892), pp. 1054–1058. Available at: https://www.sciencemag.org/lookup/doi/10.1126/science.1155371.

Schmidt, K.M. and Montgomery, D.R. 1995. Limits to Relief. *Science* 270(5236), pp. 617–620. Available at: http://www.sciencemag.org/cgi/doi/10.1126/science.270.5236.617.

Schwanghart, W. et al. 2016. Repeated catastrophic valley infill following medieval earthquakes in the Nepal Himalaya. *Science* 351(6269), pp. 147–150. doi: 10.1126/science.aac9865.

Shen, P. et al. 2020. Declining geohazard activity with vegetation recovery during first ten years after the 2008 Wenchuan earthquake. *Geomorphology* 352, p. 106989. Available at: https://doi.org/10.1016/j.geomorph.2019.106989.

Stolle, A. et al. 2017. Catastrophic valley fills record large Himalayan earthquakes, Pokhara, Nepal. *Quaternary Science Reviews* 177, pp. 88–103. Available at: https://doi.org/10.1016/j.quascirev.2017.10.015.

Stolle, A. et al. 2019. Protracted river response to medieval earthquakes. *Earth Surface Processes and Landforms* 44(1), pp. 331–341. Available at: http://doi.wiley.com/10.1002/esp.4517.

Tang, C. et al. 2012. Catastrophic debris flows on 13 August 2010 in the Qingping area, southwestern China: The combined effects of a strong earthquake and subsequent rainstorms. *Geomorphology* 139–140(August 2010), pp. 559–576. Available at: http://dx.doi.org/10.1016/j.geomorph.2011.12.021.

Tang, C. et al. 2016. Analysing post-earthquake landslide activity using multi-temporal landslide inventories near the epicentral area of the 2008 Wenchuan earthquake. *Natural Hazards and Earth System Sciences* 16(12), pp. 2641–2655. doi: 10.5194/nhess-16-2641-2016.

842 Tolorza, V. et al. 2019. Suspended Sediments in Chilean Rivers Reveal Low Postseismic Erosion
843 After the Maule Earthquake (Mw 8.8) During a Severe Drought. *Journal of Geophysical*
844 *Research: Earth Surface* 124(6), pp. 1378–1397. Available at:
845 https://onlinelibrary.wiley.com/doi/abs/10.1029/2018JF004766.

846 Turowski, J.M. and Rickenmann, D. 2009. Tools and cover effects in bedload transport
847 observations in the Pitzbach, Austria. *Earth Surface Processes and Landforms* 34(1), pp. 26–37.
848 Available at: http://doi.wiley.com/10.1002/esp.1686.

849 Vanmaercke, M. et al. 2014. Seismic controls on contemporary sediment export in the Siret river
850 catchment, Romania. *Geomorphology* 216, pp. 247–262. Available at:
851 http://dx.doi.org/10.1016/j.geomorph.2014.04.008.

852 Vanmaercke, M. et al. 2017. Exploring the effects of seismicity on landslides and catchment
853 sediment yield: An Italian case study. *Geomorphology* 278, pp. 171–183. Available at:
854 http://dx.doi.org/10.1016/j.geomorph.2016.11.010.

855 Wang, J. et al. 2015. Controls on fluvial evacuation of sediment from earthquake-triggered
856 landslides. *Geology* 43(2), pp. 115–118. doi: 10.1130/G36157.1.

857 Wang, J.J. et al. 2013. Angle of repose of landslide debris deposits induced by 2008 Sichuan
858 Earthquake. *Engineering Geology* 156, pp. 103–110. Available at:
859 http://dx.doi.org/10.1016/j.enggeo.2013.01.021.

860 Wang, W. et al. 2017. Perturbation of fluvial sediment fluxes following the 2008 Wenchuan
861 earthquake. *Earth Surface Processes and Landforms* 42(15), pp. 2611–2622. doi:
862 10.1002/esp.4210.

863 West, A.J. et al. 2014. Dilution of10Be in detrital quartz by earthquake-induced landslides:
864 Implications for determining denudation rates and potential to provide insights into landslide
865 sediment dynamics. *Earth and Planetary Science Letters* 396, pp. 143–153. Available at:
866 http://dx.doi.org/10.1016/j.epsl.2014.03.058.

867 Wilkinson, P.L. et al. 2002. An integrated hydrological model for rain-induced landslide
868 prediction. *Earth Surface Processes and Landforms* 27(12), pp. 1285–1297. doi:
869 10.1002/esp.409.

870 Williams, J.G. et al. 2018. Satellite-based emergency mapping using optical imagery: Experience
871 and reflections from the 2015 Nepal earthquakes. *Natural Hazards and Earth System Sciences*
872 18(1), pp. 185–205. doi: 10.5194/nhess-18-185-2018.

873 Yang, F. et al. 2021. Catastrophic debris flows triggered by the 20 August 2019 rainfall, a decade
874 since the Wenchuan earthquake, China. *Landslides* (October 2020). doi: 10.1007/s10346-021-
875 01713-6.

876 Yanites, B.J. et al. 2010. How rivers react to large earthquakes: Evidence from central Taiwan.
877 *Geology* 38(7), pp. 639–642. Available at:
878 http://pubs.geoscienceworld.org/geology/article/38/7/639/130315/How-rivers-react-to-large-
879 earthquakes-Evidence.

880 Yunus, A.P. et al. 2020. Decadal vegetation succession from MODIS reveals the spatio-temporal
881 evolution of post-seismic landsliding after the 2008 Wenchuan earthquake. *Remote Sensing of*
882 *Environment* 236(October 2019), p. 111476. Available at:

883   https://doi.org/10.1016/j.rse.2019.111476.

884   Zhang, F. et al. 2019. Monsoonal control on a delayed response of sedimentation to the 2008
885   Wenchuan earthquake. *Science Advances* 5(6). Available at:
886   http://advances.sciencemag.org/lookup/doi/10.1126/sciadv.aav7110.

887   Zhang, S. et al. 2014. Relationships among three repeated large-scale debris flows at Pubugou
888   Ravine in the Wenchuan earthquake zone. *Canadian Geotechnical Journal* 51(9), pp. 951–965.
889   Available at: http://www.nrcresearchpress.com/doi/abs/10.1139/cgj-2013-0368.

890   Zhang, S. and Zhang, L.M. 2017. Impact of the 2008 Wenchuan earthquake in China on
891   subsequent long-term debris flow activities in the epicentral area. *Geomorphology* 276, pp. 86–
892   103. Available at: http://dx.doi.org/10.1016/j.geomorph.2016.10.009.

893